

See discussions, stats, and author profiles for this publication at: <https://www.researchgate.net/publication/272423688>

Guanidine Nitrate Enhanced Catalysis of Nitrogen-Doped Carbon Nanotubes for Metal-Free Styrene Production through Direct Dehydrogenation

ARTICLE *in* CHEMCATCHEM · FEBRUARY 2015

Impact Factor: 4.56 · DOI: 10.1002/cctc.201402934

CITATIONS

7

READS

50

4 AUTHORS, INCLUDING:



Zhongkui Zhao

Dalian University of Technology

97 PUBLICATIONS 850 CITATIONS

[SEE PROFILE](#)



Yitao Dai

Aarhus University

14 PUBLICATIONS 77 CITATIONS

[SEE PROFILE](#)



Ge Guifang

Dalian University of Technology

7 PUBLICATIONS 22 CITATIONS

[SEE PROFILE](#)

Guanidine Nitrate Enhanced Catalysis of Nitrogen-Doped Carbon Nanotubes for Metal-Free Styrene Production through Direct Dehydrogenation

Zhongkui Zhao,* Yitao Dai, Guifang Ge, and Guiyu Wang^[a]

Nitrogen-doped carbon nanotubes (CNTs) with defect- and C=O-group-rich surface features were fabricated through a facile and scalable physical dry milling and subsequent pyrolysis approach of carbon nanotubes and melamine in the presence of guanidine nitrate. The catalytic performance of the as-prepared N-doped CNTs with diverse guanidine nitrate dosages and pyrolysis temperatures for direct dehydrogenation of ethylbenzene to styrene under oxidant- and steam-free conditions was measured. Various characterization techniques including high-resolution transmission electron microscopy, X-ray diffraction, X-ray photoelectron spectroscopy, nitrogen-adsorption and thermogravimetric analysis, and Raman spectroscopy were employed to investigate the structure and surface properties, as well as to explore the relationship between catalyst nature and catalytic performance. It is found that the addition of guanidine nitrate in the pyrolysis process of CNT with melamine significantly affects the structure, surface properties, and cata-

lytic performance. The optimized N-doped CNTs demonstrate steady-state styrene production rates 1.56 and 1.60 times higher than those of the parent CNTs and the established nanodiamond, as well as 6.49 times the rate of commercially available K-Fe catalyst without compromising the selectivity to styrene. The much superior catalytic performance in metal-free catalytic direct dehydrogenation can be ascribed to the C=O group- and defect-rich surface nature, the basic properties resulted from N-doping, the larger surface area and pore volume, and smaller graphitic carbon crystallites. The fabricated novel N-doped CNTs can be considered as a promising candidate for sustainable production of styrene through oxidant- and steam-free direct dehydrogenation of ethylbenzene with energy-saving and environmentally benign features. The developed defect-formation strategy in this work can be used for preparation of other metal-free carbocatalysts.

Introduction

Direct dehydrogenation (DDH) of ethylbenzene to styrene is one of the commercially important reactions in the chemical industry. The commercial K-Fe catalyst has some disadvantages such as quick deactivation owing mainly to potassium loss, unstable Fe³⁺ state, coke deposition, as well as health injuries to humans caused by the presence of chromium in this system. Moreover, the introduction of superheated steam into the feed is indispensable, as it provides the thermodynamic driving force of this endothermic reaction and shifts the chemical equilibrium to higher styrene conversion, besides inhibiting the quick deactivation caused by coke deposition.^[1] However, as steam is used in molar excess to ethylbenzene (\approx 2–3:1 in current technology), the amount of energy spent is relatively high.^[2] The search for new catalyst systems with high stability of Fe³⁺ species and coke resistance in the absence of potassium

or steam is highly required, but a large breakthrough on these issues cannot be expected soon although many efforts have been made.^[3] From the viewpoint of sustainable developments, carbocatalysts are considered as fascinating candidates with energy-saving, clean and safe features for styrene production. However, current efforts are mainly focused on carbon-catalyzed oxidative dehydrogenation,^[4] and reports on oxygen- and steam-free direct dehydrogenation are scarce.^[5] Therefore, the development of metal-free nanocarbon-catalyzed DDH process in the absence of oxidant and steam is highly desirable but remains a rigorous challenge.

The DDH reaction of ethylbenzene to styrene under oxygen- and steam-free conditions by using nanodiamond as an efficient metal-free catalyst was reported^[5a] and presents a promising start for studies developing carbon-based catalysts for this reaction. Recently, a core-shell sp²/sp³ composite-structured hybrid nanocarbon was demonstrated as an active and selective catalyst for DDH of propane to propene.^[5d] It was found that the optimum catalytic activity depends on the maximum structural defectiveness and high chemical reactivity of the ketone groups. We have demonstrated that the introduction of nitrogen into the carbon structure can efficiently enhance the catalytic properties including activity and selectivity for DDH of ethylbenzene to styrene under oxidant- and steam-free conditions.^[5b] The lone electron pairs of the nitrogen

[a] Prof. Z. Zhao, Dr. Y. Dai, Dr. G. Ge, Prof. G. Wang

State Key Laboratory of Fine Chemicals
Department of Catalysis Chemistry and Engineering
School of Chemical Engineering
Dalian University of Technology
Dalian 116024 (P.R. China)
Fax: (+86) 411-84986354
E-mail: zkzhao@dlut.edu.cn

 Supporting information for this article is available on the WWW under <http://dx.doi.org/10.1002/cctc.201402934>.

atoms can form a delocalized conjugated system with the sp^2 -hybridized carbon frameworks to change the electronic behavior and can also produce defect sites on the carbon surface resulting in great improvement of the reactivity,^[6] as well as the introduction of N can improve the basic properties of carbon materials resulting in promotion of the dehydrogenation activity but inhibition of cracking of ethylbenzene as a side reaction by decreasing the amount of phenolic hydroxyl groups.^[5a–c,7] We also found that a CN_x layer coated on nanodiamonds leads to much superior catalytic performance to that of the parent nanodiamond.^[5c] Carbon nanotubes(CNTs) are often described as rolled-up graphene layers, and the pristine and surface-modified forms have been demonstrated to be effective catalysts for alkenes production through oxidative dehydrogenation of their corresponding alkanes.^[4c,8] Created and enlarged structural defects on the nanocarbon surface may also promote catalytic performance.^[9] By exploring efficient and scalable approaches to make and/or enlarge surface structural defects on nanocarbon materials, our group aims at developing novel and highly efficient carbocatalysts for diverse transformations. In the approach reported herein, we envision that the catalytic properties of carbon nanotubes can be improved by N doping and defect formation, resulting in an excellent catalyst for DDH reaction.

Guanidine nitrate, a salt formed from guanidine and nitric acid, may explosively decompose while it is heated up to 150 °C. As N-doped CNTs can be fabricated by a facile pyrolysis of CNTs with melamine,^[10] it was proposed that the addition of guanidine nitrate in the pyrolysis procedure would create and/or enlarge surface structural defect leading to an excellent catalyst with enhanced catalytic performance in DDH of ethylbenzene, which was denoted G-M-CNT (Scheme 1). To the best of our knowledge, our work presents the first report on the guanidine nitrate effect and the N-doping on the material feature and catalysis of carbon materials. The as-prepared sample with the pyrolysis process but in absence of guanidine nitrate was denoted as M-CNT. By changing the mass ratio of guanidine nitrate to CNT and fixing the melamine dosage, a series of defect- and C=O-group-rich N-doped CNTs samples were prepared. The pyrolysis temperature was further optimized, and

a series G-M-CNT with diverse pyrolysis temperatures were also prepared. The obtained N-doped CNTs and the parent CNT were characterized by employing XRD analysis, high-resolution transmission electron microscopy (HRTEM), X-ray photoelectron spectroscopy (XPS), and Raman spectroscopy, and the characterization results were compared with the reaction results.

Results and Discussion

Effect of guanidine nitrate addition

The catalytic performance of the developed G-M-CNT (mass ratio of guanidine to CNT is 20:1), M-CNT, as well as the pristine CNT for metal-free carbon-catalyzed DDH reaction of ethylbenzene under oxidant- and steam-free conditions reaction was measured, and the reaction results are depicted in Figure 1. Clearly, the G-M-CNT demonstrates much superior catalytic activity (steady-state styrene rate, 3.95 mmol g⁻¹ h⁻¹, without optimization) to the pristine CNT (2.79 mmol g⁻¹ h⁻¹),

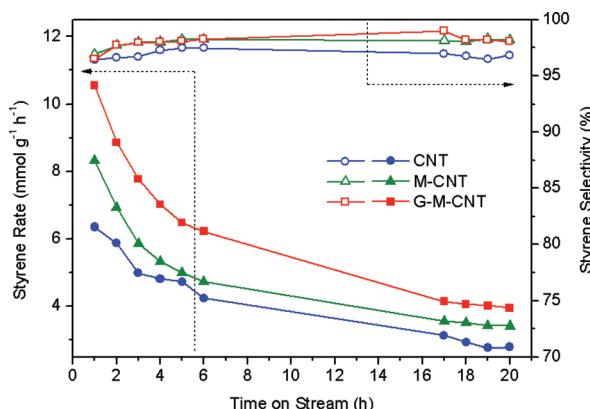


Figure 1. Catalytic performance of G-M-CNT, M-CNT, and pristine CNT as a function of time on stream for metal-free DDH of ethylbenzene to styrene under oxidant- and steam-free conditions.

and even to M-CNT(3.38 mmol g⁻¹ h⁻¹), suggesting the promoting effect of guanidine nitrate addition and N doping. To reveal the essential reason for the superior catalytic performance, the structure and surface feature of the three samples were characterized by employing HRTEM, XRD, Raman spectroscopy, and XPS techniques.

In Figure 2, typical HRTEM images of G-M-CNT, CNT, and pristine CNT are presented. As shown, in Figure 2d–f, the CN_x-layer-coating CNT hybrid structure can be formed by pyrolysis of CNT with melamine in the absence of guanidine nitrate. However, the addition of guanidine nitrate in the pyrolysis process results in CN_x layer disappearing (Figure 2g–i). In comparison with pristine CNT (Figure 2a–c), the structural defect on the G-M-CNT prepared in the presence of guanidine nitrate can be clearly observed. The disappearance of the CN_x layer on the G-M-CNT and the surface defect may be a result of the explosive decomposition of guanidine nitrate. The created and/or enlarged structural defect may promote the catalytic per-



Scheme 1. Schematic illustration of the preparation procedure of novel N-doped carbon nanotubes by a facile pyrolysis approach of carbon nanotube and melamine with the addition of guanidine nitrate.

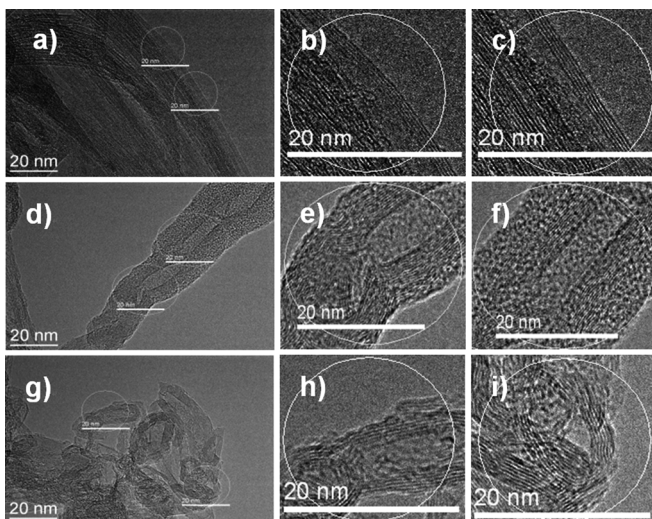


Figure 2. Typical HRTEM images of a) pristine CNT with b,c) the magnified regions marked in (a); d) M-CNT with e,f) the magnified regions marked in (d); and g) G-M-CNT with h, i) the magnified regions marked in (g).

formance of N-doped CNTs for various reactions including DDH of ethylbenzene to styrene.

The structures of the as-prepared G-M-CNT and M-CNT as well as the parent pristine were further characterized by XRD and Raman techniques (Figure 3). From Figure 3a, for G-M-CNT and pristine CNT, the diffraction peaks towards (002), (100), and (111) lattice planes can be identified,^[5b,c] indicating the well-formed graphitic structure. However, no peaks corresponding to (100) and (111) planes for M-CNT can be well resolved. Correlated to HRTEM images, the disappearance of diffraction peaks may be caused by the surface CN_x layer. Additionally, the (002) diffraction peaks appear on pristine CNT and the as-prepared G-M-CNT, the significantly broader width at half maximum for the latter can be clearly observed, suggesting smaller graphitic crystallite size, which may be favorable for higher catalytic activity for DDH reaction. Moreover, the diffraction peak corresponding to (002) plane on the XRD patterns of G-M-CNT shifts to higher diffraction angle than that of pristine CNT, indicating the smaller interlayer distance. Although the graphitic crystallite size of M-CNT is very small, the too thick surface CN_x may be unfavorable for the desired reaction. As seen in Figure 1, M-CNT still exhibits higher catalytic activity for DDH reaction, which is ascribed to N-doping into the carbon matrix confirmed by XPS analytical results. From Figure 3b, we could observe two main first-order Raman modes at approximately 1337 and 1585 cm⁻¹, corresponding to A1g mode in disordered carbon or structural defects and to E2g mode of ideal graphitic carbon for the three samples, respectively.^[11] The G peak of M-CNT also shifts from 1586 to 1577 cm⁻¹ relative to that of pristine CNT, ascribed to N incorporation into carbon matrix.^[12] However, only a slight shift from 1586 to 1583 cm⁻¹ towards the G band of G-M-CNT can be observed relative to that of pristine CNT, which shows that the guanidine nitrate addition can result in different surface structure from that of M-CNT prepared in the absence of guanidine nitrate, which was confirmed by the HRTEM and XRD

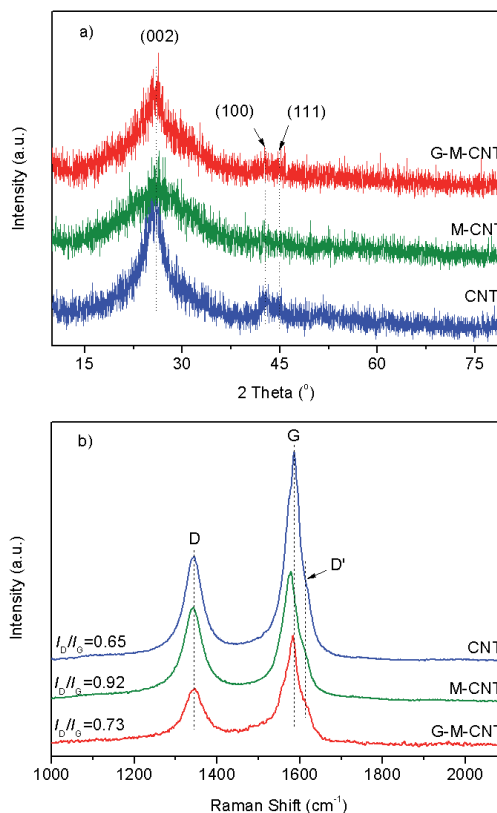


Figure 3. a) XRD patterns and b) Raman spectra of the as-prepared G-M-CNT, M-CNT, and the parent CNT.

analytical results. Furthermore, the more obvious D' peak appears as a shoulder peak of the G band in comparison to that of pristine CNT, suggesting the enlarged structural defect.^[13] The larger I_D/I_G of G-M-CNT than that of pristine CNT is also an indicator of more structural defect and lattice edges of the as-prepared hybrid composite.^[14] The enlarged structural defectiveness of G-M-CNT in comparison to pristine CNT owing to the explosive decomposition of guanidine nitrate in the pyrolysis process is consistent with the results from the above HRTEM analysis. As a result, the as-prepared G-M-CNT exhibits much superior catalytic performance in DDH reaction in comparison to pristine CNT. Although the M-CNT has the largest I_D/I_G value, the thick CN_x layer on CNT surface may be unfavorable for DDH reaction. The larger I_D/I_G for G-M-CNT than that of CNT also indicates the smaller in-plane crystallite size of G-M-CNT to parent CNT,^[14] in agreement with the result from XRD.

From above analysis, the created and/or enlarged structural defectiveness, smaller graphitic crystalline size and N atom incorporation into carbon matrix of G-M-CNT obtained by pyrolysis of CNT and melamine in the presence of guanidine nitrate may allow it to be a better catalyst for DDH reaction in comparison to parent CNT. The C=O can be the catalytic active species, which serves as Lewis bases to activate saturated hydrocarbon for this dehydrogenation reaction, and the surface phenolic hydroxyl group and/or possible COOH may enhance the cracking of ethylbenzene owing to its acidity, because acid sites are active for cracking reaction of hydrocarbon.^[5,7d] There-

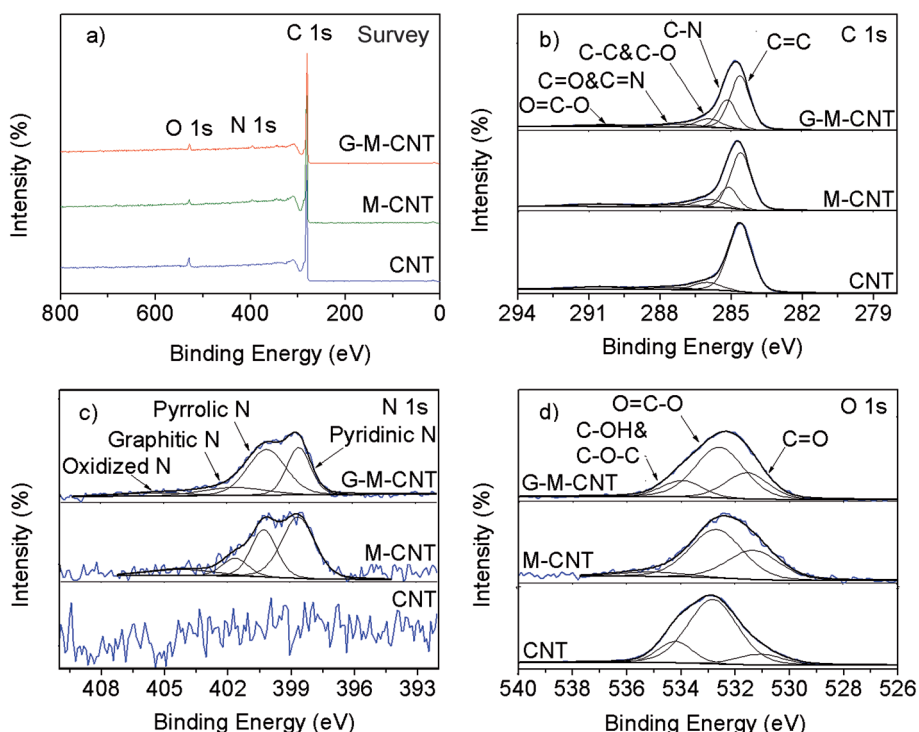


Figure 4. XPS spectra of the as-prepared G-M-CNT, M-CNT, and parent CNT. a) Survey spectra (the M-CNT and the parent CNT are included for comparison); b-d) C 1s, N 1s, O 1s, respectively.

fore, the investigation on the surface chemistry properties of the developed materials is essential. Herein, XPS analysis was performed to investigate the surface chemistry for the nature and coordination states of the carbon, nitrogen, and oxygen in the fabricated G-M-CNT, M-CNT, as well as the parent CNT (Figure 4), and the quantitative analysis results are presented in Table 1. The XPS survey spectra (Figure 4a) of the G-M-CNT and M-CNT samples display signals from C, N, and O elements, although the signals corresponding to N and O are weak. Correlated to Figure 4b,c, the N incorporation in the G-M-CNT and M-CNT can be confirmed. The C 1s peak region in the XPS spectra of the samples (Figure 4b) was deconvoluted to five peaks at approximately 284.6, 285.1, 286.0, 287.1, and 290.6 eV corresponding to C=C, C–N, C–C/C–O, C=O/C=N, and O=C=O, respectively.^[15] On the surface of CNT, no C–N or C=N group can be observed. The higher C–N on the G-M-CNT and

M-CNT surface indicates the N incorporation into the carbon matrix. The N 1s XPS peak (Figure 4c) illustrates that the N atoms in G-M-CNT and M-CNT are incorporated into the graphene lattice in a form of “pyridinic N”, “pyrrolic N”, graphitic N and oxidized N, with peaks appearing at approximately 398.6, 400.1, and 401.8, 404.1–405.3 eV,^[14a, 15a,b, 16] suggesting N incorporation but not adsorption on the surface. Furthermore, from Table 1, higher pyrrolic N content on the G-M-CNT than on M-CNT is evident, which may be one reason for the superior catalytic performance of G-M-CNT in DDH reaction. The main by-products in the catalytic DDH of ethylbenzene are benzene and toluene resulting from the cracking of ethylbenzene, which is consistent with the results reported in the literature.^[5] The

surface phenolic hydroxyl group and/or possible COOH may enhance the cracking of ethylbenzene.^[7d] The introduction of nitrogen atoms into the hybrid composite can increase the electron density of carbon materials, and, therefore, strengthen the basic properties but weaken the acidity of the catalyst, which may result in improvement of the catalytic activity for styrene production and, simultaneously, suppression of the benzene and toluene formation. The basic properties of G-M-CNT and M-CNT resulting from N-doping can improve activity and selectivity (Figure 1). The O 1s XPS spectrum can be deconvoluted into three peaks with the binding energies at approximately 531.5, 532.7, and 534.0–535.5 eV, assigned to C=O (ketonic carbonyl group), O=C–O (sum of carboxylic acid, anhydride, lactone, ester group) and C–O–C/C–OH-containing groups (Figure 4d and Table 1).^[8a] From Table 1, the total surface oxygen contents on the CNT, M-CNT, and G-M-CNT are 4.1, 1.6, and 2.8%, respectively. The pyrolysis procedure and CN_x coating leads to a decreased surface O content on M-CNT relative to that on CNT. However, the guanidine nitrate addition in the pyrolysis leads to an increase in surface O content on G-M-CNT relative to that on M-CNT. The surface C=O contents, which is the active species for DDH reaction, on the CNT, M-CNT, and G-M-CNT are 0.65, 0.50, and 0.74%, respectively. N doping by pyrolysis in the presence of guanidine nitrate may increase the amount of catalytically active sites, and therefore, the catalytic performance can be significantly improved. Moreover, compared to pristine CNT, the M-CNT shows superior catalytic performance for DDH reaction although it has a little lower surface C=O content, ascribed to the N doping.

Table 1. Relative integrated intensity of deconvoluted N 1s and O 1s XPS spectra for G-M-CNT, M-CNT, and CNT samples.

Sample	N ^[a] [%]	N-1 ^[b] [%]	N-2 ^[b] [%]	N-3 ^[b] [%]	N-4 ^[b] [%]	O ^[c] [%]	C=O [%]	C–OH/C–O [%]	O=C–O [%]
CNT	0	–	–	–	–	4.1	15.8	36.4	47.8
M-CNT	1.8	50.1	27.9	14.2	7.8	1.6	31.2	10.0	58.8
G-M-CNT	1.5	30.9	48.5	14.3	6.3	2.8	26.3	15.5	58.3

[a] The surface N content of the materials from XPS. [b] Percentage of various nitrogen species occupying in the total N content; N-1, N-2, N-3, and N-4 are denoted as pyridinic N, pyrrolic N, graphitic N, and oxidized N, respectively. [c] O atom molar percentage on the material surface from XPS analysis.

By correlating the characterization results with the catalytic reaction results, it can be concluded that the G-M-CNT prepared by a facile pyrolysis approach of CNT and melamine in the presence of guanidine nitrate demonstrates much superior catalytic performance in DDH reaction, which can be ascribed to the C=O-group- and defect-rich surface nature, the basic properties resulting from N-doping, and smaller graphitic carbon crystallites. Then the G-M-CNT were further optimized by adjusting the guanidine nitrate dosage and pyrolysis temperature.

Effect of guanidine nitrate dosage

We prepared a series of G-M-CNTs by adjusting the mass ratio of guanidine nitrate to CNT in a range of 5–40, and the catalytic reaction results are presented in Figure 5. Clearly, the steady-state styrene rate increases with the increase in guanidine nitrate dosage and the maximum styrene rate of

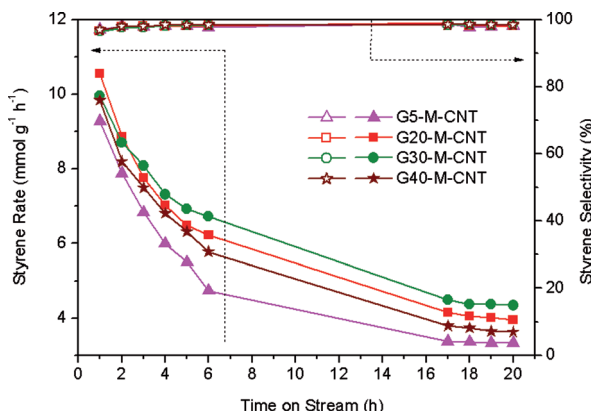


Figure 5. Catalytic performance of G-M-CNT catalysts prepared with diverse guanidine nitrate dosages as a function of time on stream for metal-free DDH of ethylbenzene to styrene under oxidant- and steam-free conditions.

4.34 mmol g⁻¹ h⁻¹ can be obtained if guanidine nitrate dosage increases up to 30, and then the catalytic activity decreases with the further increase in guanidine nitrate dosage. The mass ratio of 30:1 of guanidine nitrate to CNT is required to achieve high catalytic performance (1.56 times of the steady-state styrene rate of parent CNT). As the introduction of guanidine nitrate may decompose CN_x layers and produce structural defects, it was questioned why the further increased guanidine nitrate dosage from 30 to 40 mass ratio of guanidine nitrate to CNT results in a lower catalytic performance. HRTEM, XRD, Raman, XPS, and nitrogen adsorption techniques were employed to explore this behavior as well as the structure–performance relationship.

From Figure 6a, weakened and broadened XRD peaks corresponding to (002), (100), and (111) planes are observed upon increasing the guanidine nitrate dosage, which suggests that the increase in guanidine nitrate dosage may lead to smaller graphitic crystallite size, which may be favorable for DDH reaction.^[5b] Furthermore, the typical HRTEM images (Supporting In-

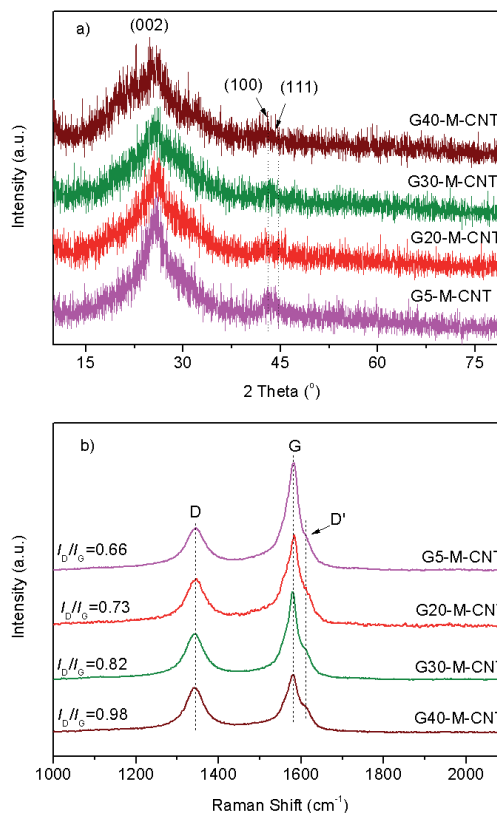


Figure 6. a) XRD patterns and b) Raman spectra of the G-M-CNT catalysts prepared with diverse guanidine nitrate dosages.

formation, Figure S1) and the Raman spectra (Figure 6b) of the G-M-CNT samples with diverse guanidine nitrate dosages indicate an enlarged structural defectiveness, and therefore the increase in guanidine nitrate dosage from 5:1 to 30:1 leads to the continuous increase in catalytic activity with similar selectivity (Figure 5). Moreover, as a CN_x layer on the G5M-CNT sample is visible (Figure S1), explosive decomposition of guanidine nitrate at 5:1 low dosage cannot completely remove the CN_x layer formed by the pyrolysis of melamine. Therefore, an appropriate guanidine nitrate dosage is required. The increase in guanidine nitrate dosage can remove CN_x layer and produce more defective sites. However, the further increase in guanidine nitrate dosage from 30:1 to 40:1 results in a decrease in the steady-state styrene yield from 4.34 to 3.55 mmol g⁻¹ h⁻¹ (Figure 5), and the further increased guanidine nitrate dosage did not lead to an increase in catalytic performance but to a decrease, although smaller graphitic crystallite size and more defective sites can be observed by HRTEM, XRD analysis, and Raman spectra. It can be proposed that the nonmonotonous change with the monotonous increase in guanidine nitrate dosage may result from the texture feature and surface chemical properties. Therefore, the nitrogen adsorption and XPS analytical experiments on the series of samples with diverse guanidine nitrate dosages were performed.

From Figure 7, it is seen that the change in guanidine nitrate dosage significantly affects the specific surface area and pore volume. With the increase of the guanidine nitrate dosage, the

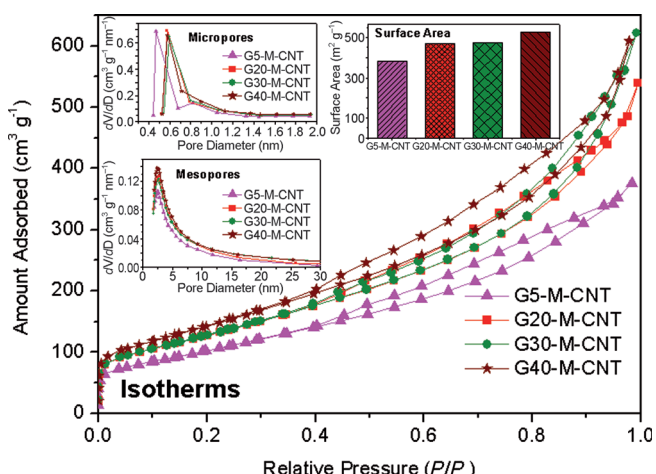


Figure 7. Nitrogen adsorption–desorption isotherms of the G–M–CNT catalysts prepared with diverse guanidine nitrate dosages. Insets: Barrett–Joyner–Halenda adsorption mesopore size distribution, Horvath–Kawazoe adsorption micropore size distribution, and specific surface area.

specific surface area and pore volume continuously increase. The micropore diameter increases as the guanidine nitrate dosage increases up to 20:1 (mass ratio of G/CNT), but no obvious change in micropore size can be observed if the dosage is further increased. Moreover, the guanidine nitrate dosage has no obvious influence on the mesopore size distribution. The change in the surface area, pore volume, and micropore diameter may be ascribed to the enlarged structural defects, confirmed by HRTEM and Raman spectroscopy. The increased

surface area and pore volume may be favorable for DDH reaction. However, upon increasing the guanidine nitrate dosage from 30:1 to 40:1, the catalytic activity does not increase but decreases, although an increased surface area from 473 to 526 m² g⁻¹ can be observed. As shown above, among the samples prepared with diverse guanidine nitrate dosage, the G40M–CNT with maximum surface area, pore volume, and structural defectiveness does not demonstrate highest catalytic performance, probably owing to the surface chemistry. Thus, XPS experiments were performed on the samples, and results are presented in Figure 8 and Table 2.

From Figure 8a and Table 2, it is seen that the increase in guanidine nitrate dosage leads to a monotonous increase in surface oxygen total content and results in an almost monotonous decrease in nitrogen content. In correlation to the reaction results, it can be found that the decreased N content, especially pyrrolic N content, is unfavorable for DDH reaction, ascribed to the decrease in basic properties and electron density, which may result in a decrease in catalytic activity for styrene production. On the other hand, the guanidine nitrate dosage has a significant influence on the distribution of different surface oxygen species (Figure 8d and Table 2). Although the increase in guanidine nitrate dosage can result in a monotonous increase in total surface oxygen content (Table 2), the continuous decrease in surface C=O percentage content in total surface oxygen can be observed as the guanidine nitrate dosage is increased. A maximum surface C=O content of 0.81% on the G30–M–CNT allows it to be an excellent catalyst with highest catalytic performance in DDH reaction. The results further prove that surface C=O is the active site for DDH reaction, and a 30:1 mass ratio of guanidine nitrate to CNT is required.

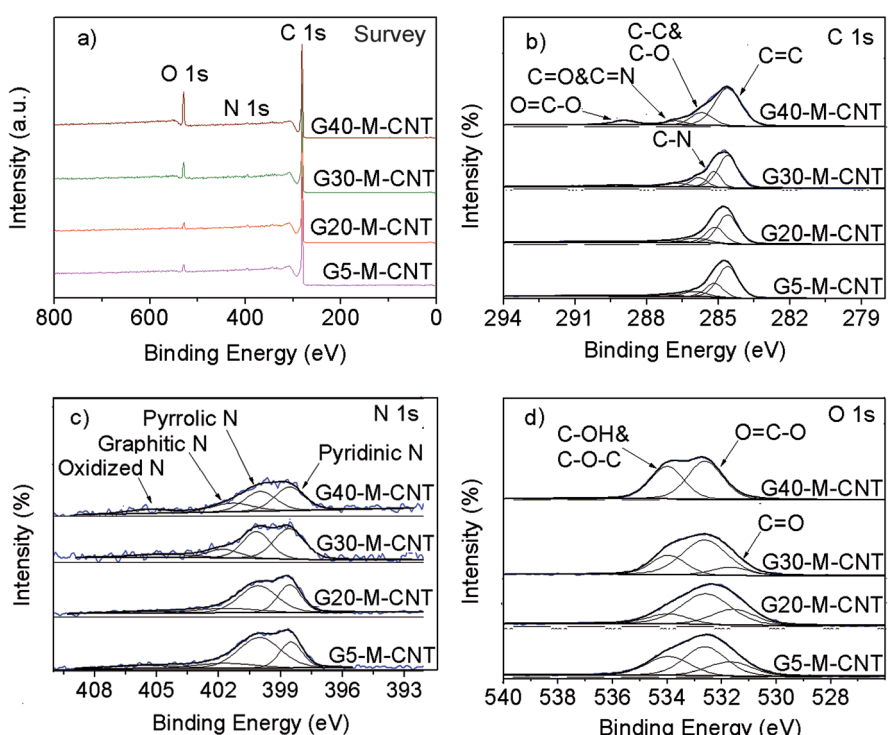


Figure 8. XPS spectra of the G–M–CNT catalysts prepared with diverse guanidine nitrate dosages. a) Survey spectra (the M–CNT and the parent CNT are included for comparison); b–d) C 1s, N 1s, O 1s, respectively.

Table 2. Relative integrated intensity of deconvoluted N 1s and O 1s XPS spectra for G-M-CNT, M-CNT, and CNT samples.

Sample	N ^[a] [%]	N-1 ^[b] [%]	N-2 ^[b] [%]	N-3 ^[b] [%]	N-4 ^[b] [%]	O ^[c] [%]	C=O [%]	C-OH/C-O [%]	O=C-O [%]
G5-M-CNT	1.7	24.5	53.5	13.0	9.1	2.6	23.9	30.3	45.8
G20-M-CNT	1.5	30.9	48.5	14.3	6.3	2.8	26.3	15.5	58.3
G30-M-CNT	1.5	42.4	34.6	13.3	9.8	6.6	12.2	25.7	62.0
G40-M-CNT	0.7	37.7	33.7	19.4	9.2	12.6	2.0	43.4	54.5

[a] Surface N content of the materials from XPS. [b] Percentage of various nitrogen species in the total N content; N-1, N-2, N-3, and N-4 are denoted as pyridinic N, pyrrolic N, graphitic N, and oxidized N, respectively. [c] O atom molar percentage on the material surface from XPS analysis.

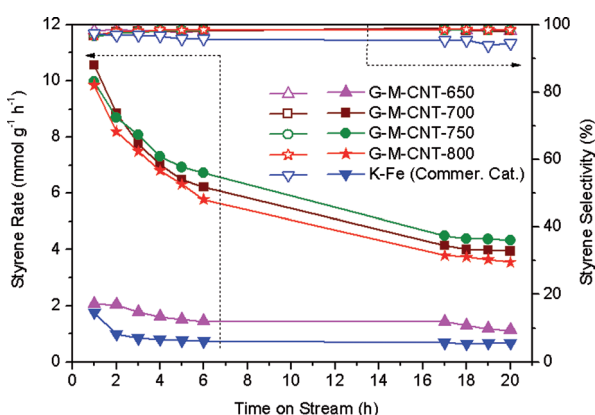


Figure 9. Catalytic performance of G-M-CNT catalysts prepared with diverse pyrolysis temperatures as a function of time on stream for metal-free DDH of ethylbenzene to styrene under oxidant- and steam-free conditions. Commer. Cat.=Commercial catalyst.

rolysis temperature. The steady-state styrene rate increases with the increase in pyrolysis temperature if it is not higher than 750 °C. The further increasing pyrolysis temperature from 750 to 800 °C leads to an obvious decrease in catalytic performance. More interestingly, the G-M-CNT-650 shows a very poor catalytic performance in DDH reaction. The 750 °C of appropriate pyrolysis temperature is required, and the 4.34 mmol g⁻¹ h⁻¹ of steady-state styrene rate can be achieved on the optimized G-M-CNT-750 sample, which exhibits a 1.59 and 6.49 times higher steady-state styrene rate than the established nanodiamond and industrially used K-Fe catalyst, respectively. Then, HRTEM, XRD and XPS experiments were performed to explore the structure–performance relationship.

From Figure S2, a very thick CN_x sheet (17.4 % of surface N content) coating on CNT can be observed on the G-M-CNT-650 sample. The CN_x sheet completely covers the CNT, and even no CNT structure can be observed. If the pyrolysis temperature is increased up to 750 °C, no CN_x layer may be observed. However, the further increase in pyrolysis temperature may lead to enlarged defectiveness, which is favorable for DDH reaction. In Figure S3 it is demonstrated that the increasing pyrolysis temperature

may lead to larger graphitic crystallite size, confirmed by the sharper XRD peaks with the higher pyrolysis temperature. From Figure S4, it is observed that the surface area, pore volume, and pore-size distribution of the G-M-CNT-650 (the 31 m² g⁻¹ lower surface area, 0.16 cm³ g⁻¹ smaller pore volume, and 55–80 nm much larger pore diameter resulted from the formed CN_x at lower pyrolysis temperature on CNT) are significantly different from those of the samples prepared with higher pyrolysis temperatures, which may be ascribed to its complete different structure and morphology from others confirmed by HRTEM images (Figure S2). The formed stacking CN_x sheets and its much lower surface area make the G-M-CNT-650 exhibit very poor catalytic performance, even worse than that of pristine CNT. As the pyrolysis temperature increases up to 700 °C, owing to the disappearance of CN_x sheets (Figure S2), the surface area and pore volume significantly rise up to 477 m² g⁻¹ and 0.82 cm³ g⁻¹, as well as the 55–80 nm pores disappear. As a result, the much superior catalytic performance of G-M-CNT-700 to that of G-M-CNT-650 can be observed. As the pyrolysis temperature is increased from 700 to 750 °C, a similar surface area, mesopore diameter but larger pore volume and micropore diameter can be observed. The further increased pyrolysis temperature up to 800 °C leads to an obvious decrease in surface area, which may depress the catalytic performance.

Furthermore, the XPS analytical results (Figure S5 and Table 3) revealed that the pyrolysis temperature notably affects the surface chemical properties. The significantly different C components on the different samples show the change in surface structural features, confirmed by HRTEM results. By comparing the three samples (G-M-CNT-650, G-M-CNT-750, and G-M-CNT-800), the increase in sp² carbon but decrease in sp³ carbon with the increasing pyrolysis temperature can be observed (Table 3), which may be one reason for the different catalytic performance. The dramatic decrease in surface N content from 17.4 to 1.5 % with the increase in pyrolysis temperature from 650 to 750 °C can be observed, the N content on the sample even decreases up to 0.3 % if the pyrolysis temperature is increased from 750 to 800 °C. From Table 3, the total oxygen contents on the G-M-CNT-650, G-M-CNT-750, and G-M-CNT-800 are 13.0, 6.6, and 19.8 %, respectively. The G-M-CNT-800 sample has the highest surface C=O content, but its catalytic

Table 3. Relative integrated intensity of deconvoluted N 1s and O 1s XPS spectra for G-M-CNT, M-CNT, and CNT samples.

Sample	N ^[a] [%]	N-1 ^[b] [%]	N-2 ^[b] [%]	N-3 ^[b] [%]	N-4 ^[b] [%]	O ^[c] [%]	C=O [%]	C-OH/C-O [%]	O=C-O [%]
G-M-CNT-650	17.4	66.5	26.4	4.0	3.1	13.0	21.6	19.8	58.6
G-M-CNT-750	1.5	42.4	34.6	13.3	9.8	6.6	12.2	25.7	62.0
G-M-CNT-800	0.3	61.5	30.1	0	8.5	19.8	24.8	10.8	64.4

[a] Surface N content of the materials from XPS. [b] Percentage of various nitrogen species occupying in the total N content; N-1, N-2, N-3, and N-4 are denoted as pyridinic N, pyrrolic N, graphitic N, and oxidized N, respectively. [c] O atom molar percentage on the material surface from XPS analysis.

performance is lower than that of G-M-CNT-750, suggesting the catalytic performance is also dependent on the structure nature (structural defectiveness, graphitic crystallite size, surface area, etc) and chemical environment (basic properties and electronic properties), besides the surface C=O content. Moreover, among the three samples (G-M-CNT-650, G-M-CNT-750, G-M-CNT-800), G-M-CNT-650 has the highest N content (17.4%) and higher surface C=O content (2.8%, calculated by surface total O content magnified by C=O percentage), but it shows much lower catalytic activity with similar selectivity than others, further confirming the catalytic performance is strongly dependent on the carbon structure, besides the surface chemical properties.

In conclusion, a significantly dropped catalytic activity during the initial period can be observed, which shows similar features to the reported results in the literature.^[5a–c] To explore the reason for this activity drop, we performed XPS, thermogravimetric analysis, and nitrogen adsorption experiments (Figure 10 and Figure S6) on the spent G-M-CNT-750. From XPS characterization results (Figure 10a,b), although the fresh and spent samples have same surface O atom content (6.6 at.-%), a decrease in the amount of surface ketonic C=O groups on the spent catalyst (4.5%) relative to that on fresh one (12.2%) can be observed, which may be ascribed to the hydrogen passivation confirmed by the increased C–OH content from 25.7 to 38.5%. As a result, the activity dropped at the initial reaction period. The above results are consistent with those reported in the literature.^[5a] From Figure 10c, the visible difference in the TG and DSC curves between fresh and spent samples can be observed, indicating the coke formation in the dehydrogenation process. The decrease in surface area and pore volume as well as increased micropore diameter further demonstrated the coke formation. Therefore, the quick drop in catalytic activity at the initial period may be ascribed to dehydrogenation process by hydrogen and coke deposition.

In Figure 11, the results of cycling DDH are presented followed by air exposure on the developed G-M-CNT-750 catalyst. We can see the catalytic activity quickly drops during the initial period but it can reach steady state by extending time on stream. More importantly, the decreased catalytic activity can be recovered by air exposure at an appropriate temperature. The remarkable steady-state activity over a long period of time and good regeneration behavior allows it to be a potential catalyst for future industrial application.

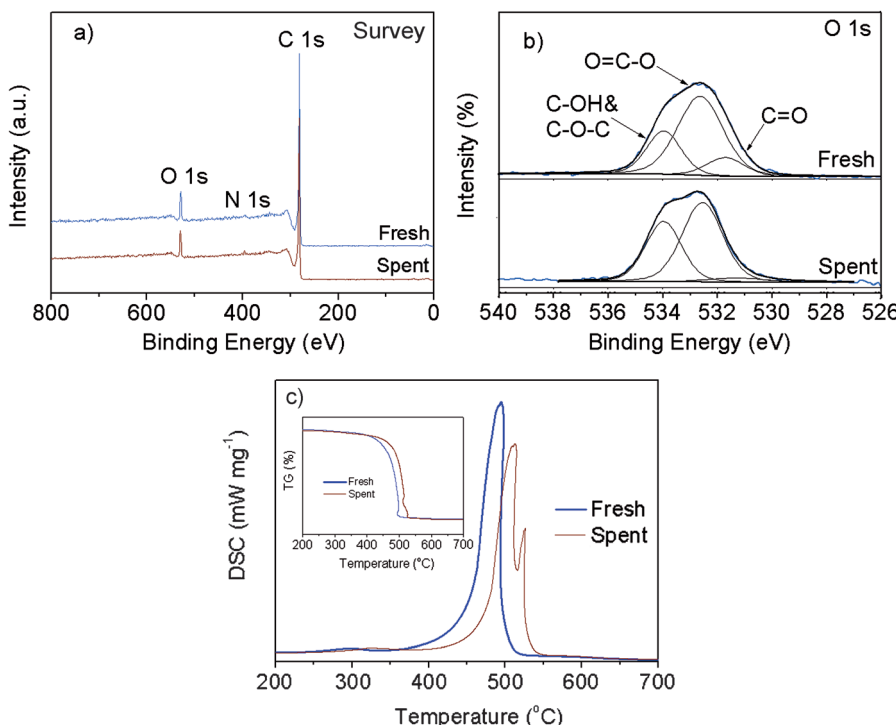


Figure 10. XPS analysis with a) survey spectra and b) O 1s spectra and c) thermogravimetry (inset) and differential scanning calorimetry curves for fresh and spent G-M-CNT-750 catalysts.

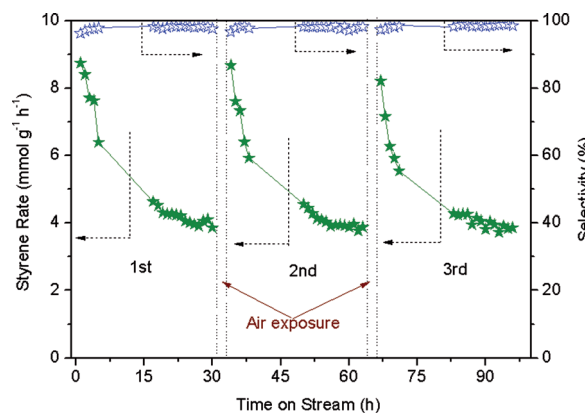


Figure 11. Catalytic performance of cycling DDH followed by air exposure on the developed G-M-CNT-750 catalyst.

Conclusions

We have developed an excellent metal-free carbocatalyst for sustainable production of styrene through direct dehydrogenation reaction by a facile and scalable pyrolysis approach of CNT with melamine in the presence of guanidine nitrate under optimized pyrolysis conditions. The outstanding catalytic properties for DDH reaction can be mainly ascribed to the C=O-group- and defect-rich surface nature, the basic properties resulting from N-doping, and smaller graphitic carbon crystallites, strongly affected by the addition of guanidine nitrate, guanidine nitrate dosage, and pyrolysis temperature. The catalytic performance of carbon materials in the direct dehydro-

generation reaction is significantly dependent on the structural nature of nanocarbon, besides on the surface chemical properties. The quick decrease in catalytic activity during the initial period may be ascribed to the dehydrogenation process by hydrogen and coke deposition. The spent catalyst can be recovered by air exposure. The fabricated novel N-doped CNT can be considered as a promising candidate for sustainable production of styrene through oxidant- and steam-free direct dehydrogenation of ethylbenzene with energy-saving and environmental benign features. The developed defect-formation strategy in this work can be used in the development of other excellent metal-free carbocatalysts for sustainable chemistry.

Experimental Section

Catalysts preparation

The commercially supplied carbon nanotubes with less than 8 nm outer diameter and 10–30 length (Chengdu Organic Chemicals Co. Ltd., Chinese Academy of Sciences, China) was washed by H_2SO_4/HNO_3 mixed aqueous solution to remove the residual metal particles. The purified CNT was used as a parent material to the prepared N-doped CNTs. The detailed preparation procedure was as follows: The CNT was finely ground with melamine in an agate mortar (1:10), in the presence or absence of guanidine nitrate and then heated up to the desired temperature in N_2 atmosphere for the pyrolysis process at a certain ramp rate to obtain the final N-doped CNTs (Scheme 1). The as-prepared N-doped CNTs in the presence and absence of guanidine nitrate are denoted as G–M–CNT and M–CNT, respectively. By changing the mass ratio of guanidine nitrate to CNT and at a fixed melamine dosage, the series of N-doped CNTs was prepared, which are denoted as G5–M–CNT, G20M–CNT, G30M–CNT, and G40M–CNT, respectively. A series of N-doped CNTs with diverse pyrolysis temperatures (G–M–CNT-650, G–M–CNT-700, G–M–CNT-750, G–M–CNT-800) were also prepared.

Catalysts characterization

X-ray diffraction (XRD) profiles were collected from 10 to 90° at a step width of 0.02° using Rigaku automatic X-ray diffractometer (D/Max 2400) equipped with a $CuK\alpha$ source ($\lambda = 1.5406 \text{ \AA}$). TEM images were obtained by using Tecnai F30 HRTEM instrument (FEI Corp.) at an acceleration voltage of 300 kV. The XPS spectra were taken on an ESCALAB 250 XPS system with a monochromatized $AlK\alpha$ X-ray source (15 kV, 150 W, 500 μm , pass energy = 50 eV). Raman spectra were measured by using a laser with an excitation wavelength of 532 nm at RT on a Thermo Scientific DXR Raman microscope. Thermogravimetric analyses experiment were performed on an SDT Q600 (V20.9 Build 20) instrument with a temperature ramp rate of $10^\circ\text{C min}^{-1}$. Nitrogen adsorption and desorption isotherms were determined on a Beishide apparatus of model 3H-2000PS1 system at -196°C . The specific surface areas were calculated by the BET method as well as the micropore and mesopore size distributions were calculated from adsorption branch of the isotherm by Horvath-Kawazoe and Barret-Joyner-Halenda model, respectively.

Catalytic performance measurement

Direct dehydrogenation of ethylbenzene was performed at 550°C for 20 h in a stainless steel fixed-bed flow reactor (6 mm O.D.). The

catalyst (25 mg) was loaded at the center of the reactor with two quartz wool plugs at its two sides. The system was heated to 600°C and kept for 30 min in Ar for pretreating the catalyst. After the system was cooled down to 550°C and kept for 10 min, the feed containing 2.8% ethylbenzene with a flow rate 10 mL min^{-1} and Ar as a balance was then fed into the reactor from a saturator kept at 40°C . The effluent from the reactor was condensed in two traps containing a certain amount of ethanol connected in a series. The condensed material was cooled externally in an ice-water bath. Quantitative analysis of the collected reaction products (ethylbenzene, styrene, toluene, and benzene) was performed on a FULI 9790 II GC equipped with an HP-5 column, $30 \text{ m} \times 0.32 \text{ mm} \times 0.25 \mu\text{m}$, and flame ionization detector. The resulting carbon balance was above $100 \pm 4\%$ in all reactions. The styrene rate and selectivity of styrene were employed as the evaluation standard for the catalytic performance of the fabricated catalysts. The styrene rate was calculated as the formed styrene molar amount per gram of catalyst per hour, and the selectivity of styrene was denoted as the percentage of the desired styrene to the total products including the desired styrene and the byproducts that contain benzene and toluene. For comparison, the catalytic properties of the parent CNT, and the industrially used K–Fe catalysts were also measured. The spent catalyst was recovered by air exposure at an appropriate temperature for a certain time.

Acknowledgements

This work is financially supported by the National Natural Science Foundation of China (grant no. 20803006 and 21276041), the Joint Fund of Coal, set up by National Natural Science Foundation of China and Shenhua Co., Ltd. (No. U1261104), and also sponsored by the Chinese Ministry of Education via the Program for New Century Excellent Talents in University (Grant no. NCET-12-0079).

Keywords: carbon • dehydrogenation • doping • nanotubes • nitrogen

- [1] a) B. D. Herzog, H. F. Raso, *Ind. Eng. Chem. Prod. Res. Dev.* **1984**, *23*, 187–196; b) M. Baghalha, O. Ebrahimpour, *Appl. Catal. A* **2007**, *326*, 143–151; c) A. C. Oliveira, J. L. G. Fierro, A. Valentini, P. S. S. Nobre, M. do C. Rangel, *Catal. Today* **2003**, *85*, 49–57; d) D. E. Stobbe, F. R. Van Buren, A. W. Stobbe-Kreemers, A. J. Van Dillen, J. W. Geus, *J. Chem. Soc. Faraday Trans.* **1991**, *87*, 1631–1637.
- [2] a) O. Shekhah, W. Ranke, A. Schle, G. Kolios, R. Schlögl, *Angew. Chem. Int. Ed.* **2003**, *42*, 5760–5763; *Angew. Chem.* **2003**, *115*, 5938–5941; b) F. Cavani, F. Trifiro, *Appl. Catal. A* **1995**, *133*, 219–239; c) W. P. Addiego, C. A. Estrada, D. W. Goodman, M. P. Rosynek, *J. Catal.* **1994**, *146*, 407–414.
- [3] a) F. Cavani, F. Trifiro, A. Vaccari, *Catal. Today* **1991**, *11*, 173–301; b) P. Kústrowski, A. Rafalska-Łasocha, D. Majda, D. Tomaszewska, R. Dziembaj, *Solid State Ionics* **2001**, *141*–*142*, 237–242; c) X. Ye, N. Ma, W. Hua, Y. Yue, C. Miao, Z. Xie, Z. Gao, *J. Mol. Catal. A* **2004**, *217*, 103–108; d) N. Mimura, I. Takahara, M. Saito, Y. Sasaki, K. Murata, *Catal. Lett.* **2002**, *78*, 125–128; e) Y. Ohishi, T. Kawabata, T. Shishido, K. Takaki, Q. Zhang, Y. Wang, K. Nomura, K. Takehira, *Appl. Catal. A* **2005**, *288*, 220–231; f) R. J. Balasamy, A. Khurshid, A. A. S. Al-Ali, L. A. Atanda, K. Sagata, M. Asamoto, H. Yahiro, K. Nomura, T. Sano, K. Takehira, S. S. Al-Khattaf, *Appl. Catal. A* **2010**, *390*, 225–231; g) O. Shekhah, W. Ranke, R. Schlögl, *J. Catal.* **2004**, *225*, 56–68.
- [4] a) C. Su, K. P. Loh, *Acc. Chem. Res.* **2013**, *46*, 2275–2285; b) L. F. Wang, J. Zhang, D. S. Su, Y. Y. Ji, X. J. Cao, F. S. Xiao, *Chem. Mater.* **2007**, *19*, 2894–2897; c) J. Zhang, X. Liu, R. Blume, A. Zhang, R. Schlögl, D. S. Su, *Science* **2008**, *322*, 73–77; d) N. Xiao, Y. Zhou, Z. Ling, Z. Zhao, J. Qiu,

- Carbon* **2013**, *60*, 514–522; e) L. Liu, Q. F. Deng, B. Agula, X. Zhao, T. Z. Ren, Z. Y. Yuan, *Chem. Commun.* **2011**, *47*, 8334–8336; f) C. Liang, H. Xie, V. Schwartz, J. Howe, S. Dai, S. H. Overbury, *J. Am. Chem. Soc.* **2009**, *131*, 7735–7741; g) R. Rao, M. Yang, Q. Ling, C. Li, Q. Zhang, H. Yang, A. Zhang, *Catal. Sci. Technol.* **2014**, *4*, 665–671; h) P. Niebrzydowska, R. Janus, P. Kuśtrowski, S. Jarczewski, A. Wach, A. M. Silvestre-Albero, F. Rodríguez-Reinoso, *Carbon* **2013**, *64*, 252–261.
- [5] a) J. Zhang, D. S. Su, R. Blume, R. Schlögl, R. Wang, X. Yang, A. Gajović, *Angew. Chem. Int. Ed.* **2010**, *49*, 8640–8644; *Angew. Chem.* **2010**, *122*, 8822–8826; b) Z. K. Zhao, Y. T. Dai, J. H. Lin, G. R. Wang, *Chem. Mater.* **2014**, *26*, 3151–3161; c) Z. K. Zhao, Y. T. Dai, *J. Mater. Chem. A* **2014**, *2*, 13442–13451; d) R. Wang, X. Sun, B. Zhang, X. Sun, D. Su, *Chem. Eur. J.* **2014**, *20*, 6324–6331.
- [6] a) Y. Zheng, Y. Jiao, Y. L. Ge, M. Jaroniec, S. Z. Qiao, *Angew. Chem. Int. Ed.* **2013**, *52*, 3110–3116; *Angew. Chem.* **2013**, *125*, 3192–3198; b) Y. Zhao, L. Yang, S. Chen, X. Wang, Y. Ma, Q. Wu, Y. Jiang, W. Qian, Z. Hu, *J. Am. Chem. Soc.* **2013**, *135*, 1201–1204.
- [7] a) Y. Wang, X. Wang, M. Antonietti, *Angew. Chem. Int. Ed.* **2012**, *51*, 68–89; *Angew. Chem.* **2012**, *124*, 70–92; b) N. Brun, S. A. Wohlgemuth, P. Osiceanu, M. M. Titirici, *Green Chem.* **2013**, *15*, 2514–2524; c) X. Jin, V. V. Balasubramanian, S. T. Selvan, D. P. Sawant, M. A. Chari, G. Q. Lu, A. Vinu, *Angew. Chem. Int. Ed.* **2009**, *48*, 7884–7887; *Angew. Chem.* **2009**, *121*, 8024–8027; d) Y. V. Kissin, *Catal. Rev.* **2001**, *43*, 85–146; e) J. Lu, L. Yang, B. Xu, Q. Wu, D. Zhang, S. Yuan, Y. Zhai, X. Wang, Y. Fan, Z. Hu, *ACS Catal.* **2014**, *4*, 613–621.
- [8] a) W. Qi, W. Liu, B. Zhang, X. Gu, X. Guo, D. Su, *Angew. Chem. Int. Ed.* **2013**, *52*, 14224–14228; *Angew. Chem.* **2013**, *125*, 14474–14478; b) B. Frank, M. Morassutto, R. Schomäcker, R. Schlögl, D. Su, *ChemCatChem* **2010**, *2*, 644–648; c) Y. Marco, L. Roldan, E. Munoz, E. Garcia-Bordeje, *ChemSusChem* **2014**, *7*, 2496–2504; d) W. Qi, D. Su, *ACS Catal.* **2014**, *4*, 3212–3218; e) V. Zarubina, H. Talebi, C. Nederlof, F. Kapteijn, M. Makkee, I. Melian-Cabrera, *Carbon* **2014**, *77*, 329–340.
- [9] a) C. Su, M. Acik, K. Takai, J. Lu, S. Hao, Y. Zheng, P. Wu, Q. Bao, T. Enoki, Y. J. Chabal, K. P. Loh, *Nat. Commun.* **2012**, *3*, 1298; b) Y. Gao, D. Ma, C. Wang, J. Guan, X. Bao, *Chem. Commun.* **2011**, *47*, 2432–2434; c) D. E. Resasco, *Nat. Nanotechnol.* **2008**, *3*, 708–709; d) J. Zhu, A. Holmen, D. Chen, *ChemCatChem* **2013**, *5*, 378–401.
- [10] a) Z. Wang, R. Jia, J. Zheng, J. Zhao, L. Li, J. Song, Z. Zhu, *ACS Nano* **2011**, *5*, 1677–1684; b) S. Wang, E. Iyyamperumal, A. Roy, Y. Xue, D. Yu, L. Dai, *Angew. Chem. Int. Ed.* **2011**, *50*, 11756–11760; *Angew. Chem.* **2011**, *123*, 11960–11964.
- [11] a) Y. Xia, R. Mokaya, *Chem. Mater.* **2005**, *17*, 1553–1560; b) V. N. Khabashesku, J. L. Zimmerman, J. L. Margrave, *Chem. Mater.* **2000**, *12*, 3264–3270; c) R. Silva, J. Al-Sharab, T. Asefa, *Angew. Chem. Int. Ed.* **2012**, *51*, 7171–7175; *Angew. Chem.* **2012**, *124*, 7283–7287.
- [12] a) Y. Xia, R. Mokaya, *Adv. Mater.* **2004**, *16*, 1553–1558; b) M. B. Ansari, B. H. Min, Y. H. Mo, S. E. Park, *GreenChem.* **2011**, *13*, 1416–1421; c) Y. Mao, H. Duan, B. Xu, L. Zhang, Y. Hu, C. Zhao, Z. Wang, L. Chen, Y. Yang, *Energy Environ. Sci.* **2012**, *5*, 7950–7955.
- [13] C. Han, A. Doepeke, W. Cho, V. Likodimos, A. A. de La Cruz, T. Back, W. R. Heineman, H. B. Halsall, V. N. Shanov, M. J. Schulz, P. Falaras, D. D. Dionysiou, *Adv. Funct. Mater.* **2013**, *23*, 1807–1816.
- [14] a) Z. Lin, G. Waller, Y. Liu, M. Liu, C. P. Wong, *Adv. Energy Mater.* **2012**, *2*, 884–888; b) P. Wu, Y. Qian, P. Du, H. Zhang, C. Cai, *J. Mater. Chem.* **2012**, *22*, 6402–6412; c) H. Muramatsu, K. Fujisawa, Y. I. Ko, K. S. Yang, T. Hayashi, M. Endo, C. M. Yang, Y. C. Jung, Y. A. Kim, *Chin. J. Catal.* **2014**, *35*, 864–868.
- [15] a) J. Y. Kim, W. H. Lee, J. W. Suk, J. R. Potts, H. Chou, I. N. Kholmanov, R. D. Pineri, J. Lee, D. Akinwande, R. S. Ruoff, *Adv. Mater.* **2013**, *25*, 2308–2313; b) C. Zhang, L. Fu, N. Liu, M. Liu, Y. Wang, Z. Liu, *Adv. Mater.* **2011**, *23*, 1020–1024; c) Y. Li, Y. Zhao, H. Cheng, Y. Hu, G. Shi, L. Dai, L. Qu, *J. Am. Chem. Soc.* **2012**, *134*, 15–18; d) N. Jung, S. Kwon, D. Lee, D. M. Yoon, Y. M. Park, A. Benayad, J. Y. Choi, J. S. Park, *Adv. Mater.* **2013**, *25*, 6854–6858; e) L. Shang, T. Bian, B. Zhang, D. Zhang, L. Z. Wu, C. H. Tung, Y. Yin, T. Zhang, *Angew. Chem. Int. Ed.* **2014**, *53*, 250–254; *Angew. Chem.* **2014**, *126*, 254–258.
- [16] a) W. Ding, Z. Wei, S. Chen, X. Qi, T. Yang, J. Hu, D. Wang, L. J. Wan, S. F. Alvi, L. Li, *Angew. Chem. Int. Ed.* **2013**, *52*, 11755–11759; *Angew. Chem.* **2013**, *125*, 11971–11975; b) G. Wu, N. H. Mack, W. Gao, S. Ma, R. Zhong, J. Han, J. K. Baldwin, P. Zelenay, *ACS Nano* **2012**, *6*, 9764–9776; c) X. H. Li, S. Kurasch, U. Kaiser, M. Antonietti, *Angew. Chem. Int. Ed.* **2012**, *51*, 9689–9692; *Angew. Chem.* **2012**, *124*, 9827–9830.

Received: November 20, 2014

Revised: December 25, 2014

Published online on February 17, 2015